The Competition between Martensite and Omega in Quenched Ti-Nb Alloys

D. L. MOFFAT and D. C. LARBALESTIER

A careful experimental study of the phase transformations which occur in annealed β phase Ti-Nb alloys during quenching has been completed. The competition of the α'' and ω phases to form in alloys of 20 to 70 at. pct Nb was investigated as a function of quench rate and alloy composition. Particular attention was paid to the interstitial content and chemical homogeneity of the alloys. The martensitic α'' phase was found only in 20 and 25 at. pct Nb alloys, and then only using fast water quenches of ~300 °C/sec. Under slower quench conditions, *e.g.*, ~0.3 to 3 °C/sec, ω phase precipitates were found in these alloys and in 30 and 35 at. pct Nb alloys. Evidence of "diffuse" ω phase precipitation was observed in alloys up to 50 at. pct Nb. Only alloys of 60 and 70 at. pct Nb were found to retain the single phase β structure upon quenching. These results constitute the first part of a study of the stable and metastable equilibria of the Ti-Nb alloy system.

I. INTRODUCTION

IT generally has been accepted that only two martensitic structures exist in the Ti-Nb alloy system. These structures, α' and α'', have been observed in several other titanium-based transition element alloys.[1,2] The structure of α' is hcp[1,3,4] with lattice parameters identical to those of α-Ti. The α'' structure is C-centered orthorhombic with a Cmcm space group.[1,3-6] Hatt and Rivlin[6] and Pattanayak *et al.*[7] have reported the presence of a tetragonal phase in 25 and 21.7 at. pct Nb alloys, respectively; however, the identification of this phase as martensitic is uncertain.

The α'' structure may be viewed as being a transition from the hcp structure of α' to the bcc structure of the β phase. The atom positions in α'' are $(0, 0, 0)$, $(1/2, 1/2, 0)$, $(0, 1 - 2y, 1/2)$, and $(1/2, 1/2 - 2y, 1/2)$ with y being approximately 0.2 in Ti-Nb alloys.[4,8] By varying b/a, c/a, and y, all three structures may be produced.[4] For example, an ideal hcp structure is obtained when $y = 1/6, b/a = \sqrt{3}, c/a = \sqrt{8/3}$. A bcc structure is obtained when $y = 1/4, b/a = \sqrt{2}, c/a = \sqrt{2}$. A compilation of the existing lattice parameter data for the α' and α'' martensites is shown in Figures 1(a), (b), and (c). These data indicate that the α'/α'' "boundary" occurs at 7.2 at. pct Nb. A linear extrapolation of the data toward the bcc limit suggests that, at room temperature, the upper compositional boundary for α'' should be 30.7 at. pct Nb. The data of Morniroli and Gantois[4] for alloys of 25 to 28 at. pct Nb, however, do not follow this extrapolation.

The M_S data for the Ti-Nb system are given in Figure 2. The calculation of Kaufman and Bernstein[9] of $T_0^{\beta \to \alpha}$ is also shown. Flower *et al.*[10] noted that since there were two martensites, there should exist two M_S curves, but the scatter in the data is too great to distinguish them. Extrapolation of the data indicates that alloys of 26, 30.5, and 32 at. pct Nb should have M_S temperatures of 273, 77, and 0 K, respectively. The upper compositional limit of α'' as extrapolated from the lattice parameter data (~31 at. pct Nb) is in fair agreement with the composition having an estimated M_S of 0 K. However, the M_S extrapolation conflicts with the report that the 26.6 and 28.2 at. pct Nb alloys of Morniroli and Gantois were martensitic at room temperature.

It is noteworthy that no experimental measurements of M_S below 200 °C or for alloy compositions greater than 20 at. pct Nb have been reported. One reason given for this is that below 300 °C the thermal arrest signal becomes too small to observe.[11,12] It is also apparent in Figure 2 that increasing the niobium content much beyond 25 at. pct would lower M_S to room temperature or below. An additional complication is that the microstructures of alloys in the 20 to 30 at. pct Nb range are greatly affected by quench rate, as will be demonstrated in this paper.

The effect of quench rate on the type of transformation was studied by Jepson *et al.*[3] Their data are summarized in Figure 3. In the *nucleation and growth* region it was proposed that the thermal arrests were due to α nuclei forming by diffusion. For alloys and quench rates in the region labeled *shear*, M_S was found to be independent of quench rate. By chemically thinning specimens to 130 to 50 μm, Jepson *et al.* were able to effect extremely high quench rates which were found to suppress the martensitic transformation. The retained β phase could be transformed readily to $\beta + \alpha''$ with deformation. The possibility exists, however, that the thinning process introduced significant hydrogen contamination, which may have altered the phase transformations.

Other investigations have shown that the quenched microstructures of 14 to 30 at. pct Nb alloys are more complicated than those proposed by Jepson *et al.* Hatt and Rivlin[6] observed that furnace cooling a 20.7 at. pct Nb alloy at 0.03 °C/sec resulted in the precipitation of the ω phase. Air cooling this alloy yielded the same results. Only water quenching produced α''. Morniroli and Gantois[4] noted similar results in alloys with more than 14 at. pct Nb. Thus, it may be that the thermal arrests observed by Jepson *et al.* in the *nucleation and growth* region were actually due to the precipitation of ω, not α.

Precipitates of the ω phase have been observed in alloys of titanium and zirconium with several other transition elements. The ω phase is hexagonal and has lattice parameters which are related to the β phase lattice, *i.e.*, $a_\omega = \sqrt{2}\, a_\beta$,

D. L. MOFFAT, formerly a Graduate Student in the Materials Science Program at the University of Wisconsin–Madison, is a Research Associate in the Laboratory of Nuclear Studies, Cornell University, Ithaca, NY 14853-5001. D. C. LARBALESTIER is a Professor in the Materials Science Program, the Department of Metallurgical Engineering, and the Applied Superconductivity Center at the University of Wisconsin–Madison, Madison, WI 53706

Manuscript submitted July 13, 1987.

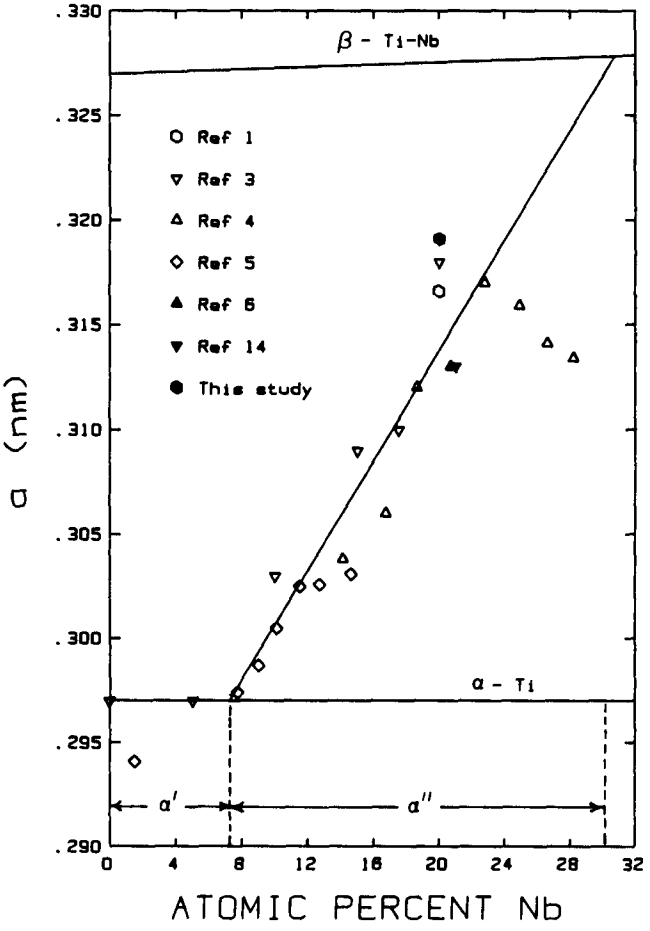

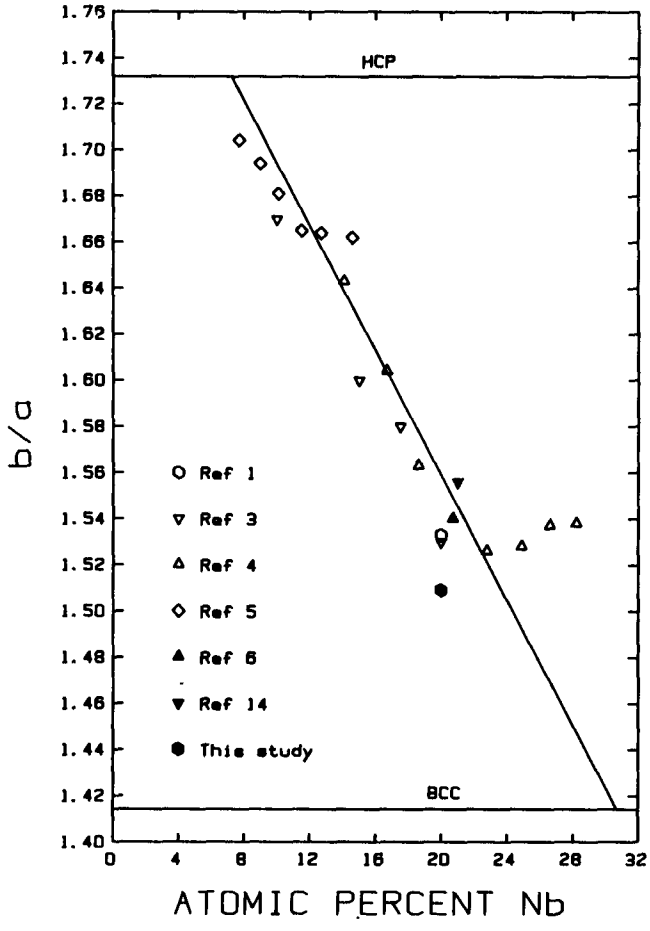

Fig. 1—The lattice parameters of the martensitic phases of Ti-Nb alloys (from the literature).

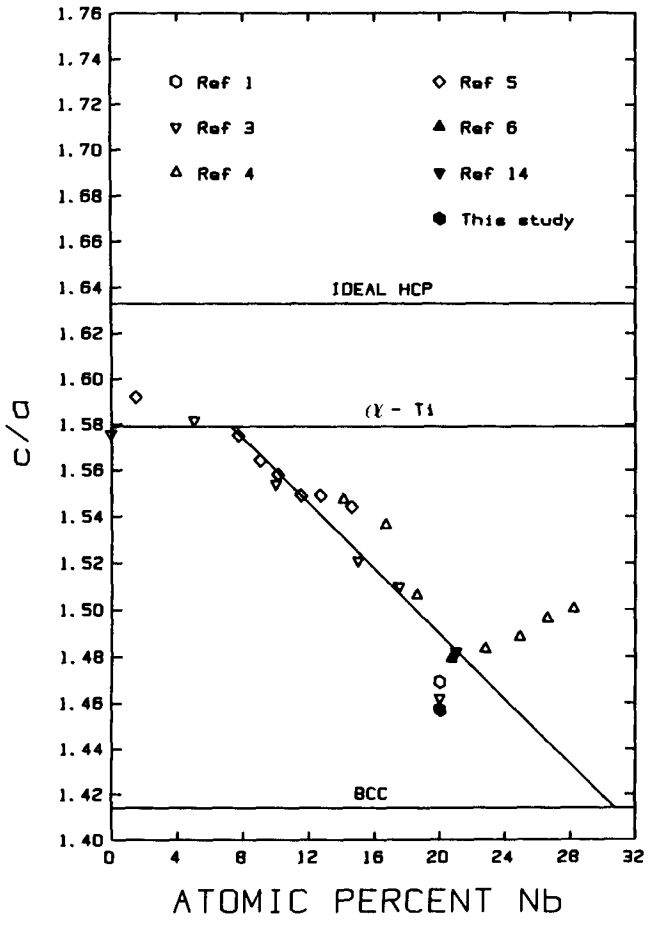

$c/a = \sqrt{3/8}$. Athermal ω precipitates have been observed in Ti-Nb alloys with compositions between 14 and 30 at. pct Nb.[4,6,13–17] The composition of athermal ω precipitates in a 21.7 at. pct Nb alloy was shown to be the same as that of the β matrix.[17]

The ω phase is formed when two of every three $\{222\}\beta$ planes collapse toward each other a distance of $\sqrt{3}\,a_\beta/12$ in the $\langle 111\rangle\beta$ direction.[18] The temperature dependence of the crystal structure of an ω precipitate formed during quenching has been described theoretically by Cook.[19–22] In this theory, the collapse of the $\{222\}\beta$ planes is described by a single Landau order parameter, η, where $\eta = 0$ gives the bcc structure and $\eta = 1$ yields ω. Upon cooling below some temperature, T_M, η abruptly changes from zero to some positive value less than one, yielding a trigonal ω phase crystal structure. Further cooling causes η to approach one. Alloy composition has been shown to have a similar effect on the crystal structure of athermal ω precipitates.[16] The process of athermal ω phase precipitation has been shown to be reversible with temperature,[23,24] provided that atomic diffusion does not alter the local composition, "locking-in" the ω structure.

The effect of quench rate on the formation of ω has not been studied explicitly. Past studies have reported only the type of quench used and the quench temperature. Balcerzak and Sass[16] noted that increasing the temperature from which the quench occurred promoted the precipitation of ω

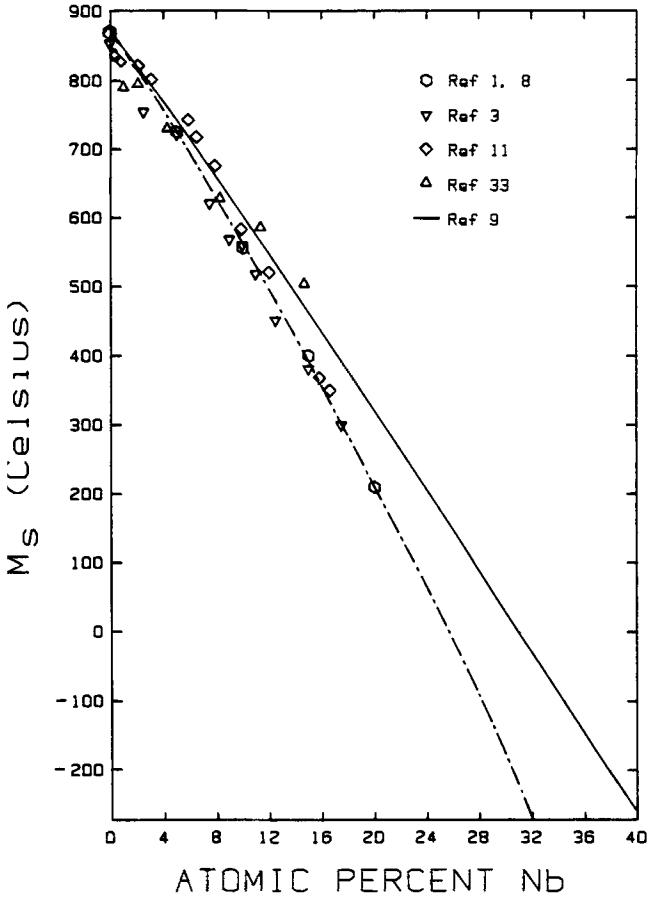

Fig. 2—The M_S data and calculations of T_0 for Ti-Nb alloys (from the literature).

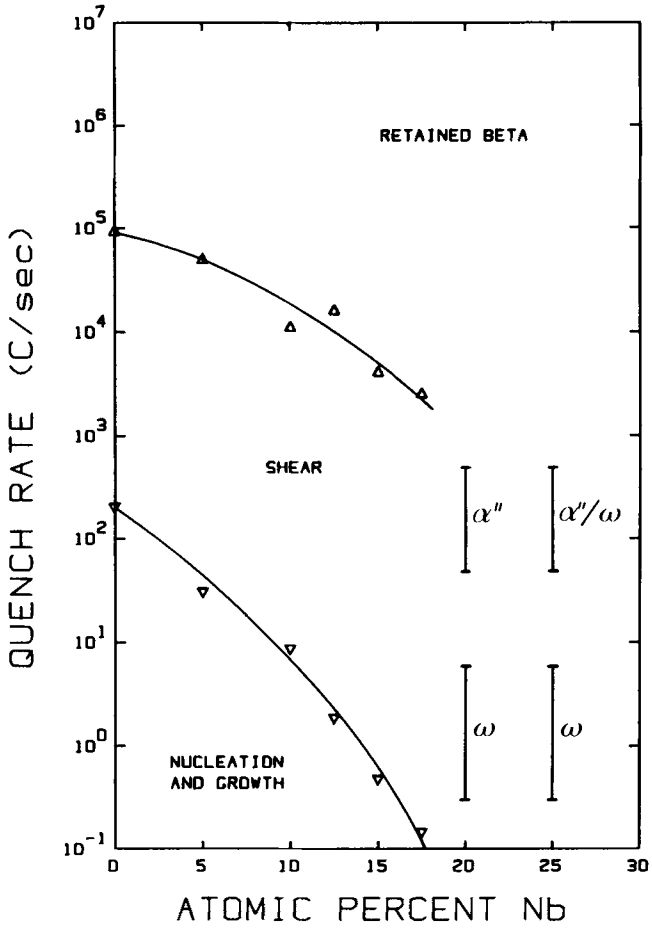

Fig. 3—Critical quench rates for Ti-Nb alloys from Ref. 3. The phases observed in the alloys of the present study after the FW and AC quenches are included for comparison.

over the formation of α. There has been no report of the measurement of an Ω_S temperature in the Ti-Nb alloy system, although there has been one in the Zr-Nb system.[25]

In summary, the general nature of the phase transformations which occur during the quenching of β phase Ti-Nb alloys is known. The details, however, are uncertain and a thermodynamic basis for these transformations is lacking. For example, it is not known if the reports of a third, tetragonal martensite are correct. The upper compositional limit of α'' formation is uncertain, as is the M_S extrapolation. The lack of an observed M_S below 200 °C raises the possibility that a competing phase transformation, such as the $\beta \rightarrow \omega$ transformation, precludes the martensitic one. There also is little agreement as to the quench rate dependence of the transformation products. Since these alloys are the most widely used superconducting materials and also find important uses in aerospace applications, it is important that the phase relationships in this alloy system be understood. This report on quenched alloys is part of a recent investigation of the phase transformations which occur in the Ti-Nb binary alloy system.[26] Particular attention has been paid to the interstitial impurity content and chemical homogeneity of the alloys used. The phase transformations which occur during isothermal aging, the underlying stable and metastable phase diagrams, and the effects of these phase transformations on the superconducting and other physical properties of these alloys will be reported in later papers.

II. EXPERIMENTAL DETAILS

A. *Alloy Fabrication*

The raw materials used to prepare the alloys in the present study were 3 mm diameter rods of niobium and 1.6 mm diameter rods of titanium. Both elements were of commercial purity (see Table I). To remove any surface oxidation, the rods were etched in a solution of 13 pct HF, 20 pct HNO_3, and 67 pct H_2O. The etched rods were rinsed several times with methanol, dried, and then stored in a desiccator until needed. Alloy ingots were arc-melted with a tungsten electrode on a water-cooled copper base. Before each melt, a titanium getter was melted to purify the argon atmosphere. The ingot was melted and inverted at least 10 times in a square depression, assuring a macroscopically homogeneous ingot. The ingot then was shaped into a cylinder roughly 1 cm in diameter. This ingot, which could be supported by the copper base in such a way that cooling was not very efficient, was carefully heated to just below the solidus, effecting a very high temperature homogenization heat treatment. The ingot was rolled over and this process repeated several times, producing a homogeneous ingot. (This was verified using SEM and EPMA techniques on several test ingots.) Each ingot was weighed after melting to monitor the change in overall composition. The worst-case errors, calculated by assuming that the material lost was either all niobium or all titanium, are shown in Table II.

Table I. Impurity Analyses of the Etched Niobium and Titanium

	C	N	O	H
Niobium	<232 (<30)	212 (32)	348 (60)	<460 (<5)
Titanium		143 (42)	1882 (630)	1138 (24)

Values in appm (wppm).

Table II. Melt Analyses of the Alloy Compositions

Nominal	Actual	Worst-Case Errors	
20	20.00	+0.005	−0.005
25	25.01	+0.015	−0.025
30	30.03	+0.075	−0.095
35	35.00	+0.180	−0.165
40	39.99	+0.215	−0.165
50	49.98	+0.325	−0.165
60	60.00	+0.305	−0.100
70	70.06	+0.540	−0.120

All percentages in at. pct Nb.

Even under these worst-case conditions, only one alloy could have deviated from its nominal composition by more than 0.5 at. pct.

After weighing, the ingots were homogenized again to remove any residual microscopic inhomogeneities. Each ingot was wrapped in niobium foil and sealed in a silica tube with several pieces of titanium rod under 20 kPa (150 torr) of argon. The ingots were homogenized at 1300 °C. The 50, 60, and 70 at. pct Nb alloys were homogenized for 24 hours; all others were homogenized for 8 hours. No detectable inhomogeneity was visible using several methods of analysis: back-scattered electron imaging in a scanning electron microscope, electron probe microanalysis, and microscopic etching. These techniques, used collectively, have been shown to reveal local inhomogeneities of ±1 at. pct.[27]

Following homogenization, the ingots were quenched by breaking the tubes under water. This was done to minimize the precipitation of the ω phase which could have made the swaging of some of the ingots difficult. The ingots were swaged to 3 mm rods without difficulty, using an area reduction of about 20 pct on each pass.

At this point analyses of interstitially dissolved elements were obtained for all the alloys. It was discovered that the quench after the homogenization heat treatment had introduced significant quantities of hydrogen into the alloys. To remove this hydrogen, the 3 mm rods were vacuum annealed at 800 °C. The annealing time was 3 hours, during which time the vacuum was $\sim 9 \times 10^{-4}$ Pa ($\sim 7 \times 10^{-6}$ torr). A section of each alloy was analyzed for impurities after this anneal. The results are shown in Table III. The hydrogen levels before this anneal were from 7 to 17 times higher than the levels reported in Table III. The carbon, nitrogen, and oxygen levels, on the other hand, varied by only ±10 pct. The total impurity content of the alloys can be seen to range from 0.27 at. pct to 0.55 at. pct. This may appear to be unacceptably high but it should be emphasized that these are atomic percentages, not the customarily reported weight percentages. (The same range in weight percentages is 0.05 pct to 0.12 pct.)

It is unclear at what level interstitial impurities influence the phase transformation in the Ti-Nb system. Most phase transformation studies reported in the literature do not give a sufficient accounting of interstitials to permit any definite conclusions to be drawn. In the present work, the effects of varying the interstitial content of the alloys were not explicitly studied. It is known, however, that these alloys are very easily contaminated by interstitials and that commercial fabrication processes pay particular attention to their control.[28] The interstitial contents of the alloys of the present study are typical of those found in commercially produced superconductors.

B. *Heat Treatment and Quenching Procedures*

The 3 mm alloy rods were cut into 25 mm lengths for the phase transformation investigations. After cleaning, the sample and two titanium getters were sealed in a silica tube under ~1 Pa (~10 mtorr) of argon. The sealed rods were solution annealed and recrystallized at 1000 °C. The 20 to 35 at. pct Nb alloys were annealed for 8 hours, the 40 to 70 at. pct alloys for 24 hours. Following this heat treatment they were quenched to room temperature.

Three different quench rates were used in the present study. A fast water quench (FW) was produced by quickly taking a tube from the furnace and breaking it under water. Removing a tube from the furnace and placing it on a table resulted in an air cool quench (AC). (It should be noted that air cooling was equivalent to taking a tube from the furnace and quenching it in water, but not breaking it.) The slowest quench, furnace cooling (FC), was produced by turning off the furnace and allowing the specimen to cool with the furnace.

As noted earlier, quenching a hot Ti-Nb alloy into water can lead to appreciable hydrogen contamination. Thus, it

Table III. Impurity Analyses after the Vacuum Anneal

Pct Nb	C	N	O	H	Total
20	755 (160)	445 (110)	2903 (820)	1068 (19)	5171 (1109)
25	785 (160)	193 (46)	3019 (820)	993 (17)	4990 (1043)
30	865 (170)	257 (59)	3821 (1000)	546 (9)	5489 (1238)
35	739 (140)	181 (40)	2774 (700)	692 (11)	4386 (891)
40	656 (120)	211 (45)	1930 (470)	456 (7)	3253 (642)
50	526 (90)	186 (37)	1580 (360)	418 (6)	2710 (493)
60	746 (120)	203 (38)	1634 (350)	<371 (<5)	2954 (513)
70	791 (120)	249 (44)	2425 (490)	<393 (<5)	3858 (659)

Values in appm (wppm).

should be expected that the FW samples will contain more hydrogen than the AC and FC samples. It is not known to what extent the FW quench contaminated the specimens, nor to what extent any additional hydrogen may have affected the quenched microstructures.

The specimen used to measure the quench rates was a length of alloy rod through which a #78 (0.41 mm) hole had been diametrically drilled. The junction of a Pt/Pt-13 pct Rh thermocouple was centered in this hole. (Initially, chromel/alumel thermocouple wires were used; however, it was found that the thermocouple wires wetted the alloy rod at 1000 °C and dissolved completely.) The leads were placed in shallow grooves in the sides of the rod, fed through a very fine alumina insulator, and then out one end of a silica tube. This end was sealed with epoxy. After the epoxy had hardened, the other end of the tube was sealed under vacuum. Cooling curves were recorded on a chart recorder. The experimentally measured quench rates are shown in Figure 4. The different quenches varied in rate by about three orders of magnitude, being ~300 °C/sec for the FW quench and ~0.3 °C/sec for the FC quench.

C. *Transmission Electron Microscopy*

TEM specimens were cut with a low speed diamond saw from the mid-section of a heat treated length of 3 mm diameter rod. The disks were ultrasonically cleaned, ground on both sides with 320 grit SiC abrasive paper until they were ~200 μm thick, and then ultrasonically cleaned again. TEM foils were prepared in a twin jet electropolisher commercially produced by E. A. Fischione. A solution of 2 pct HF, 5 pct H_2SO_4, 93 pct methanol was used at −40 to −50 °C. Immediately upon perforation, the foil was removed from the solution and thoroughly rinsed with methanol. The foils were stored in air. A JEOL 200 CX-II operating at 200 kV was used to examine the foils.

This specimen preparation technique ensured that the observed phase transformations were representative of the pure, bulk alloys as only the very center of a disk was thinned to electron transparency. This is particularly important for TEM specimens because the area examined is extremely small. For comparison, the TEM specimens of many studies have been punched from a thin sheet, and then heat treated and electropolished.

An inevitable concern when electropolishing Ti-Nb alloys is the introduction of hydrogen from the electrolyte. Even though the specimens were polished at −50 °C in a very dilute solution of HF, the foils were susceptible to contamination because of their extreme thinness. Interstitial hydrogen can, in principle, produce two effects in a TEM specimen — it can remain in solid solution, expanding the bcc lattice, or it can lead to the precipitation of hydrides. Nothing could be done in the present study to avoid examination of the material which may have contained dissolved hydrogen because such material was impossible to identify. Hydride precipitation, though infrequently observed, was easily recognizable. Because hydrides formed at the edge of the hole in a TEM foil, observations were made in somewhat thicker regions of the foil. The difficulty of preventing hydrogen charging during electropolishing causes some concern about the results of Jepson *et al.*[3] based on chemically thinned specimens, and about the identification of a tetragonal martensite.[6,7]

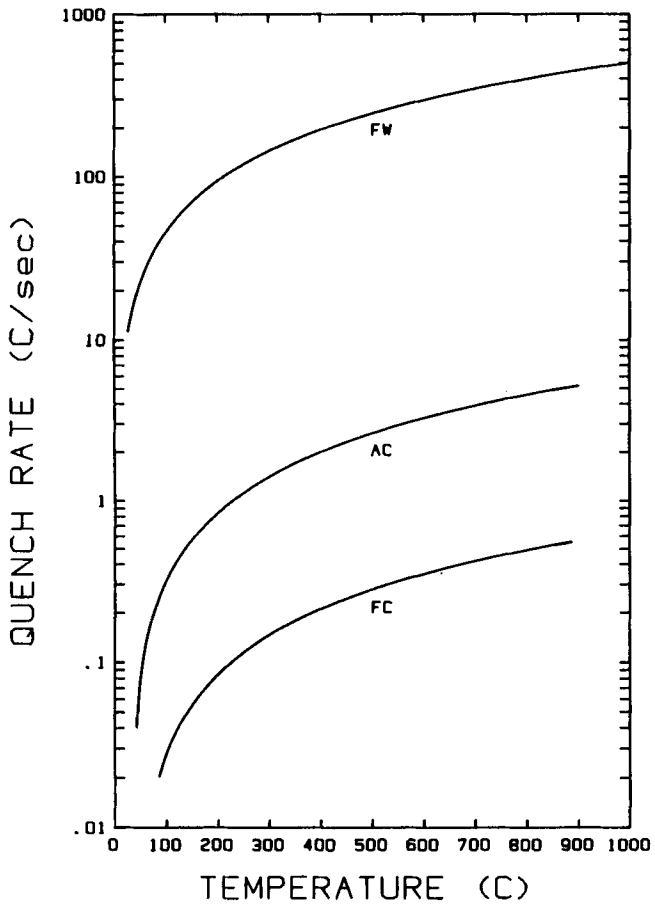

Fig. 4 — Measured quench rates for the three quenches used in this study.

D. *X-Ray Diffraction*

X-ray diffraction studies of the 20 at. pct Nb specimen were complicated by the metastable nature of the microstructures. It was found that powders of this alloy did not retain the martensitic microstructure through the filing and annealing processes. In order to obtain some information about the martensite, a solid specimen was used. A short length of 3 mm rod was cut from the 20 at. pct Nb alloy, annealed at 1000 °C and FW quenched, and then round-rolled until it was ~0.5 mm in diameter. This wire was sealed in a quartz tube under argon and annealed for 2 hours at 1000 °C.

The FW quench was difficult to produce in the wire specimen. It was undesirable to quench such a small specimen directly into water because of the possibility of further contamination. It was found, however, that a residual argon atmosphere of 13 kPa (100 torr), coupled with quenching the tube into liquid nitrogen, without breaking it, produced a martensitic specimen.

The X-ray diffraction patterns were recorded on film in a 114.6 mm diameter Debye-Scherrer camera. Nickel-filtered copper radiation was used and the exposure time was 8 hours. The values used for the wavelengths in the calculations of *d*-spacings were K_α = 0.154171 nm, $K_{\alpha 1}$ = 0.154044 nm, $K_{\alpha 2}$ = 0.154426 nm.

III. RESULTS

A. *Microstructures Resulting from Fast Water Quenching*

The FW quench produced a martensitic structure in 20 and 25 at. pct Nb alloys. A selected area diffraction (SAD) pattern and bright-field micrograph from the 20 at. pct specimen are shown in Figures 5(a) and (b). The $\beta + \alpha''$ diffraction pattern is very similar to the $\beta + \alpha$ pattern. The bright-field image shows a strained and heavily faulted microstructure. Large regions of single phase β were quite common in the 20 at. pct TEM specimen. These β regions showed no evidence of ω phase precipitation, though there was some very slight reciprocal lattice streaking in the ω positions. Light metallography indicated that the perimeter of the 25 at. pct Nb specimen had transformed to martensite, while the center appeared to be single phase β. Using TEM, very fine ω phase precipitates were found in a β matrix in the center of this specimen.

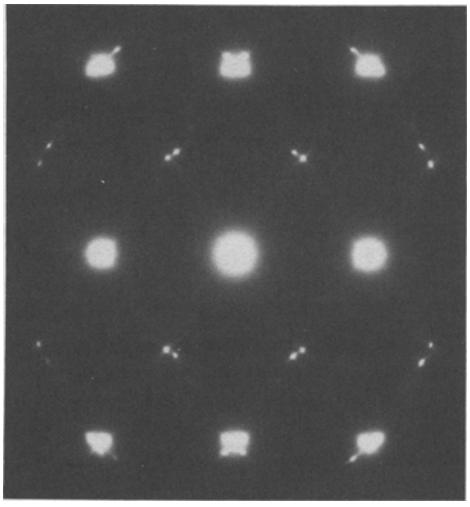

(*a*)

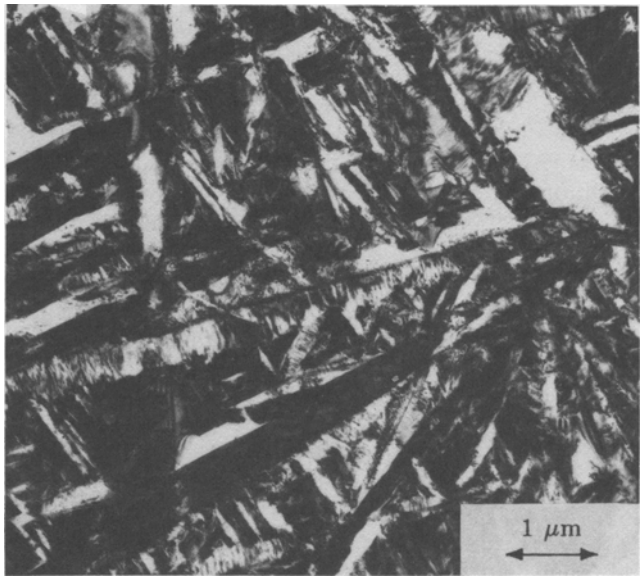

(*b*)

Fig. 5—TEM micrographs of the 20 at. pct Nb FW specimen. (*a*) SAD pattern showing β and α'' reflections. Zone axes are $[110]\beta$ and $[0001]\alpha''$. (*b*) Bright-field image.

The 30 and 35 at. pct Nb specimens were found to be single phase β. SAD patterns from these specimens, however, showed some reciprocal lattice streaking. This streaking, which is the result of the bcc structural instability, has been referred to previously in the literature as indicating the presence of "diffuse" ω. A piece of the 30 at. pct specimen was mounted in diallyl phthalate, polished, and then submerged in liquid nitrogen in an attempt to produce a martensitic structure. No rumpling of the specimen surface was observed after warming the specimen to room temperature.

The *d*-spacings determined for the 20 at. pct Nb wire specimen are given in Table IV. Due to the bulk of the specimen, absorption of the Cu K_α X-rays caused the low angle diffraction lines to be shifted significantly. Using a Nelson-Riley extrapolation, the β phase lattice parameter was calculated to be 0.32834 nm. The orthorhombic lattice parameters were determined to be $a = 0.3191$ nm, $b/a = 1.509$, $c/a = 1.457$.

B. *Microstructures Resulting from Air Cooling*

Air cooling allowed the formation of ω phase precipitates in many of the alloys. The presence of ω precipitates could be detected clearly in SAD patterns. SAD patterns from the AC specimen series are shown in Figure 6. An indexed pattern is shown in Figure 6(b). Two points concerning these patterns should be noted. The ω reflections observed in a $(110)\beta$ pattern are due to only two of the four ω variants. Double diffraction of the ω patterns from the matrix reflections produces the forbidden $(1\bar{1}00)\omega$ and $(2\bar{2}00)\omega$ reflections.[29] The extra reflections marked '+' in Figure 6(b), however, occur when the pattern of one of the ω variants is doubly diffracted from a reflection of the other ω variant. Multiply diffracted spots could be observed in the 20 and 25 at. pct specimens.

The ω diffraction spots were most intense in the 20 at. pct Nb specimen and gradually became less sharp as the niobium content increased. Using these spots, the ω precipitates in the 20 and 25 at. pct specimens could be imaged in dark field. The intensities of the ω reflections in the SAD pattern of the 30 at. pct AC specimen were insufficient to produce a dark-field image, though these reflections were sharper and more intense than those of the 30 at. pct FW specimen. The other specimens appeared to be single phase β, though considerable reciprocal lattice streaking was observed in specimens with compositions of up to 50 at. pct Nb. As in the 30 and 35 at. pct FW specimens, this streak-

Table IV. *d*-Spacings of the 20 At. Pct Nb FW Wire Specimen

d (nm)	HKL (α'')	HKL (β)	*d* (nm)	HKL (α'')	HKL (β)
0.26287	110		0.13061	202	
0.25247			0.12710	221	
0.23693	020		0.12125	132	
0.22868	111	110	0.11559	004	220
0.21114	021		0.11478	222	
0.16539	022		0.10357	310	310
0.16317		200	0.09554	043	
0.15829	200		0.09458		222
0.14222	130		0.09366	204	
0.13576	131		0.08764		321
0.13312	113	211	0.07737		330

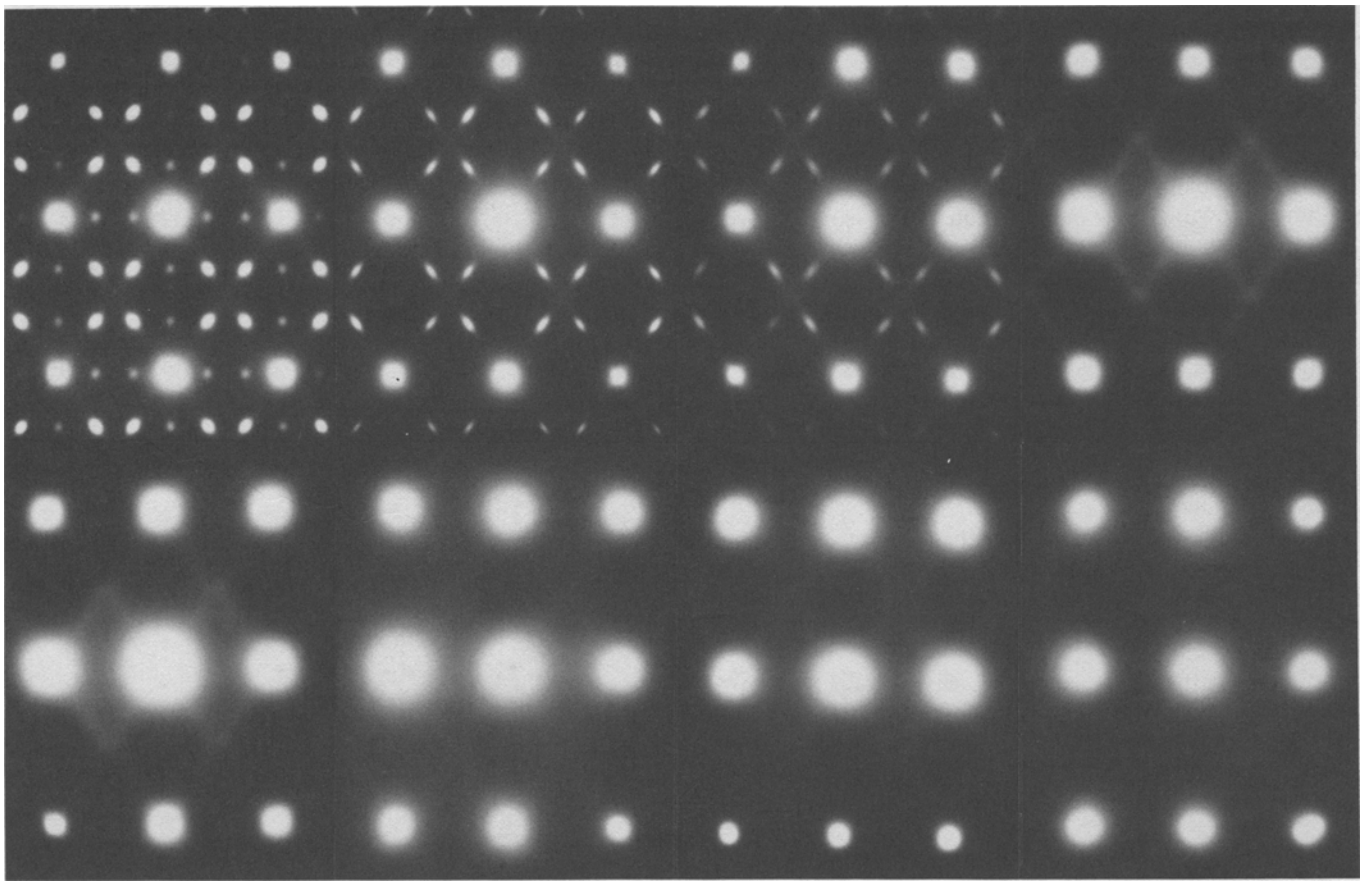

(*a*)

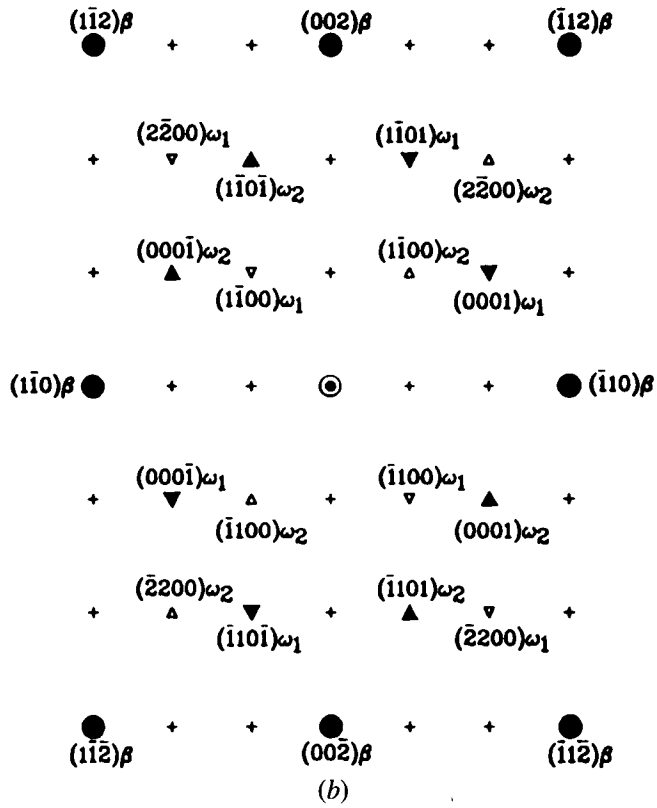

(*b*)

g. 6—SAD patterns of the AC specimens showing the change in ω phase precipitation from "real" to "diffuse". Zone axes are [110]β and [11$\bar{2}$0]ω. (*a*) Top w, left-right: 20, 25, 30, 35 at. pct Nb. Bottom row, left-right: 40, 50, 60, 70 at. pct Nb. (*b*) An indexed diffraction pattern.

ing indicated the presence of "diffuse" ω precipitates. (It should be noted that in order to show this streaking the SAD patterns of the 35 to 70 at. pct specimens were exposed ~10 times longer than those of the 20 to 30 at. pct specimens.)

Representative micrographs of the 20 to 30 at. pct Nb specimens are shown in Figures 7(a), (b), and (c). Figure 7(a) is a dark-field micrograph of the 20 at. pct AC specimen showing dense precipitation of very small ω precipitates. It should be remembered that these precipitates represent only ¼ of the total ω phase precipitation.

The bright-field micrographs in Figures 7(b) and (c) show a very different type of precipitate. Extensive tilting of the specimen did not produce any additional reflections in SAD, nor did it cause the appearance of these precipitates to change appreciably. The precipitates are visible in bright field due to the large strain fields surrounding each. These strains indicate that the precipitates are at least semicoherent with the matrix.

Polished bulk specimens of the air cooled 20 and 25 at. pct Nb alloys were submerged in liquid nitrogen in an attempt to produce a martensitic structure. As before, no surface rumpling was observed after warming the specimens to room temperature.

The X-ray diffraction pattern of the 20 at. pct Nb AC wire specimen was complex. The diffraction pattern indicated a two-phase structure, but the second phase could not be indexed as ω. The d-spacings determined for this specimen are given in Table V.

C. *Microstructures Resulting from Furnace Cooling*

The general microstructural features of the AC specimen series were reproduced in the FC specimen series. The slower cooling resulted in sharper and more intense ω phase reflections in the SAD patterns of the specimens, particularly in the 35 at. pct specimen. The precipitate/matrix interfaces in the FC specimens were more sharply defined than in the AC specimens. The slow furnace cooling also enhanced the growth of the ω precipitates.

IV. DISCUSSION

A summary of the microstructures of the quenched alloys is given in Table VI. The second phases found in the specimens as a function of alloy composition and quench rate are presented in this table (the matrix phase in all cases is β). The results show that the sensitivity of the microstructure of an alloy to quench rate increased with increasing titanium content.

The conditions under which martensite could be produced in the alloys of the present study are in general agreement with those established in the literature. A fast water quench produced α'' in specimens of the 20 and 25 at. pct Nb alloys, though the microstructure in the center of the 25 at. pct FW specimen was not martensitic. No evidence of a martensitic transformation, *i.e.*, surface rumpling, was observed in the 30 at. pct FW specimen which had been submerged in liquid nitrogen. This can be interpreted as indicating that M_S for this alloy is below 77 K if it is assumed that no reversion occurred on return to room temperature. These results are in accord with the M_S extrapolation shown in Figure 2.

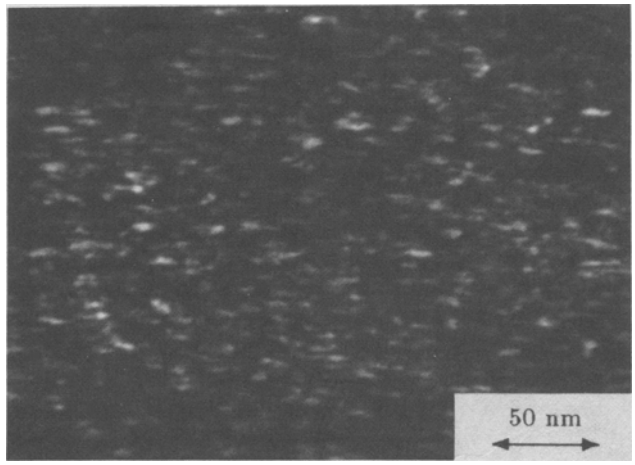

(*a*)

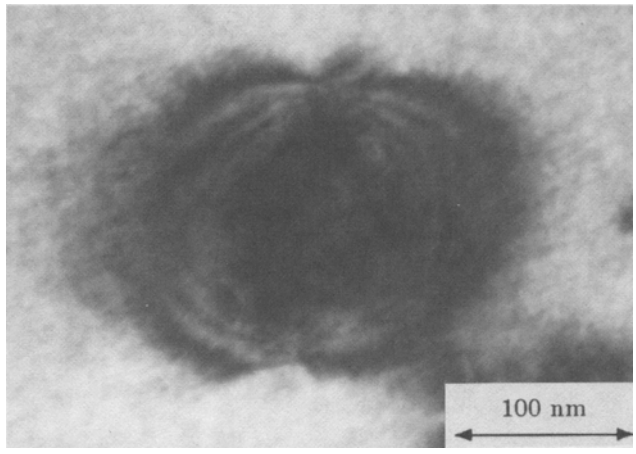

(*b*)

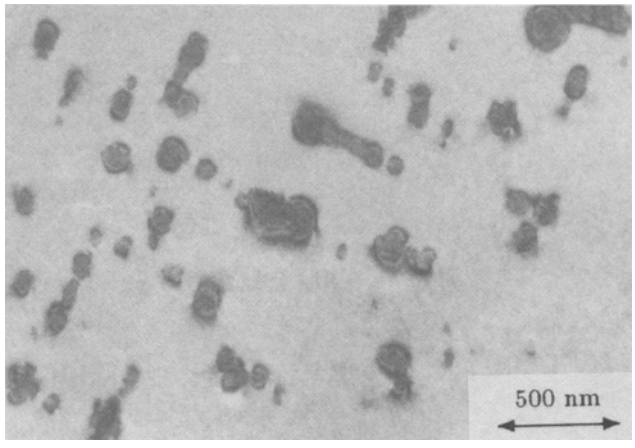

(*c*)

Fig. 7—TEM micrographs of the 20 at. pct Nb AC specimen. (*a*) Dark-field image showing athermal ω precipitates. Beam direction is $\langle 110 \rangle \beta$. (*b*) and (*c*) Bright-field images showing the unidentified precipitates. Beam direction is $\langle 120 \rangle \beta$.

When the 20 to 35 at. pct Nb alloys were quenched slowly to room temperature, the resulting microstructure was $\beta + \omega$. Comparison of the diffraction patterns of the AC and FC specimens indicated that the slower the quench, the more complete was the collapse of the $\{222\}\beta$ planes to

Table V. *d*-Spacings of the 20 At. Pct Nb AC Wire Specimen

d (nm)	HKL (β)	*d* (nm)	HKL (β)
0.28086		0.13623	
0.25378		0.13353	211
0.22972	110	0.11576	220
0.21902		0.10369	310
0.21026		0.09467	222
0.20494		0.08770	321
0.16334	200	0.08769	321
0.15061		0.08208	400
0.14604		0.08206	400
0.14202		0.07739	330
0.14013		0.07739	330

Table VI. Second Phases Observed in the Quenched Alloys

Quench	20	25	30	35
FW	α''	α''/ω	"diffuse" ω	"diffuse" ω
AC	ω	ω	ω	"diffuse" ω
FC	ω	ω	ω	ω
Quench	40	50	60	70
AC	"diffuse" ω	"diffuse" ω	none	none

Alloy compositions in at. pct Nb.
Alloys quenched from 1000 °C to room temperature.

form the hexagonal ω structure. The ω precipitates also grew larger with the slower cooling. These results may be attributed to diffusion which was enhanced by quenching at slower rates.

The dependence of the microstructure in these alloys on quench rate demonstrates two points. First, it indicates that both the $\beta \rightarrow \alpha''$ and the $\beta \rightarrow \omega$ transformations are thermodynamically allowed over a broad range of alloy compositions. Second, it shows that the favored transformation is determined by kinetics. The quench rate also determines the extent of diffusion possible during a quench, which may alter the athermal nature of the $\beta \rightarrow \omega$ transformation. Thus, it can be seen that alloy composition is a necessary, but not sufficient, condition for the formation of martensite. This is perhaps most clearly illustrated in the 25 at. pct FW specimen, which may be visualized best as being two specimens differentiated by quench rate. The quench rate at the perimeter of the specimen was fast enough to permit the formation of martensite. At the center it was slow enough to enable ω precipitates to form.

Not only do α'' and ω compete to form in an unstable matrix, but when either forms it is to the exclusion of the other. The fact that there was no evidence of a martensitic transformation in the 20 and 25 at. pct Nb AC specimens even after they had been submerged in liquid nitrogen demonstrates that ω phase precipitates prevent the formation of α''. The opposite was also shown to be true in the 20 at. pct FW specimen in which no evidence of ω phase precipitation was observed in the large β phase regions of the martensitic microstructure.

Comparison of these results to those in the literature shows two discrepancies. Figure 3 shows the type of transformation to be expected for a given quench rate according to Jepson *et al.*[3] Also shown in this figure are the FW and AC quench rates of the present study plotted for the 20 and 25 at. pct alloys. Extrapolating the data of Jepson *et al.*, the FW and AC quenches should have produced a martensitic structure in the 20 at. pct alloy. The AC quench in the 25 at. pct alloy should have produced martensite, while the FW quench may have produced single phase β. The origin of these disagreements remains unclear, though they may be related to the extreme thinness and possible hydrogen contamination of the specimens used by Jepson *et al.*

The second discrepancy concerns the α'' lattice parameter data of Morniroli and Gantois.[4] Data were given by these authors for alloys with compositions of 25, 26.6, and 28.2 at. pct Nb. These data do not fall on the linear extrapolation of the other data in Figure 1. It must be assumed, since it was not stated, that these data were obtained at room temperature. However, no other studies have reported martensite in alloys containing more than 25 at. pct Nb. Since the predicted M_S temperature for 25 at. pct Nb is about 50 °C, which is consistent with the present observations, it is questionable that these three alloys of Morniroli and Gantois were martensitic. Their anomalous lattice parameter data thus await further verification.

The ω phase could be produced in most of the alloys of the present study under the appropriate quench conditions. The 60 and 70 at. pct Nb alloys most closely approached being truly single phase. It was found that decreasing the niobium content of an alloy made it increasingly more difficult to produce a completely single phase alloy, regardless of quench rate. This is a consequence of the increasing instability of the bcc lattice.

The compositional dependence of ω phase precipitation in slowly quenched Ti-Nb alloys may be understood using the theory of Cook if it is assumed that T_M is a function of alloy composition. For pure niobium, T_M is well below room temperature. Increasing the titanium content of an alloy causes T_M to increase, eventually reaching room temperature between 35 and 40 at. pct Nb, the limit of observed athermal ω phase precipitation. At this point, η would be positive, but less than one, resulting in a trigonal ω phase crystal structure. Increasing the titanium content further would result in a greater undercooling as T_M rises above room temperature, causing η to approach one and the ω crystal structure to approach the ideal hexagonal structure. The effect of this refinement of the ω crystal structure is shown in the sequence of SAD patterns in Figure 6. Similar results have been reported for the Ti-Nb[16] and Ti-V[30] systems.

Identification of the precipitates shown in the bright-field micrographs of Figures 7(b) and (c) was not possible using SAD. Due to their asymmetrical shape, it is unlikely that these were precipitates of β', the product of a β phase miscibility gap. Similar precipitates have been seen in alloys of different compositions.[31,32]

V. CONCLUSIONS

The effects of alloy composition and quench rate on the microstructure of quenched Ti-Nb alloys were investigated in detail in the present study. Alloys of eight different compositions in the range of 20 to 70 at. pct Nb were carefully prepared and characterized. These alloys were subjected to three different rates of quench from 1000 °C to room temperature. The resulting microstructures were investigated

using light metallography, transmission electron microscopy, and X-ray diffraction.

The results can be summarized as follows:

1. As the temperature of any β phase alloy is decreased, the instability of the bcc lattice increases. The α'' and ω phases compete to form in a sufficiently unstable lattice. The mode of β phase decomposition is determined by quench rate. The two modes of decomposition are locally mutually exclusive.
2. The formation of α'' is favored by fast quench rates, *i.e.*, ~300 °C/sec, in alloys of 25 at. pct Nb or less. The M_S temperature of the 25 at. pct alloy appeared to be slightly above room temperature. Evidence of a martensitic transformation was not found in the 30 at. pct FW specimen, even after cooling it to 77 K.
3. Precipitation of the ω phase is favored by slow quench rates, on the order of ~3 °C/sec. The slower the quench, the more complete is the collapse of the $\{222\}\beta$ planes and the larger are the ω precipitates.
4. Increasing the niobium content of an alloy increases the stability of the bcc lattice at any temperature. Precipitates of the ω phase could be imaged in the 20 to 30 at. pct Nb AC and 20 to 35 at. pct Nb FC specimens. Evidence for "diffuse" ω was observed in the SAD patterns of all of the 40 and 50 at. pct specimens, regardless of quench rate, and of the 30 and 35 at. pct Nb FW specimens. The microstructures of the 60 and 70 at. pct specimens were the closest to being truly single phase.

ACKNOWLEDGMENTS

The assistance of J. Goddard, who printed the TEM micrographs and helped prepare specimens for heat treatment, is greatly appreciated. Funding for this work was provided through DOE, Division of High Energy Physics and the Wisconsin Utilities Research Foundation.

REFERENCES

1. A. R. G. Brown and K. S. Jepson: *Mém. Sci. Rev. Métall.*, 1966, vol. 63(6), pp. 575-84.
2. E. W. Collings: *The Physical Metallurgy of Titanium Alloys*, ASM, Metals Park, OH, 1984.
3. K. S. Jepson, A. R. G. Brown, and J. A. Gray: *The Science, Technology and Application of Titanium*, R. I. Jaffee and N. E. Promisel, eds., Pergamon Press, 1970, pp. 677-90.
4. J. P. Morniroli and M. Gantois: *Mém. Sci Rev. Métall.*, 1973, vol. 70(11), pp. 831-42.
5. Yu. A. Bagariatskii, G. I. Nosova, and T. V. Tagunova: *Sov. Phys.-Doklady*, 1958, vol. 3, pp. 1014-18.
6. B. A. Hatt and V. G. Rivlin: *Brit. J. Appl. Phys.*, 1968, vol. 1(2), pp. 1145-49.
7. D. Pattanayak, B. Obst and U. Wolfsteig: *Z. Metall.*, 1981, vol. 72(7), pp. 481-86.
8. A. R. G. Brown, D. Clark, J. Eastabrook, and K. S. Jepson: *Nature*, 1964, vol. 210, pp. 914-15.
9. L. Kaufman and H. Bernstein: *Computer Calculations of Phase Diagrams*, Academic Press, New York, NY, 1970.
10. H. M. Flower, R. Davis, and D. R. F. West: *Titanium and Titanium Alloys: Scientific and Technological Aspects*, Plenum Press, New York, NY, 1982, vol. 3, pp. 1703-15.
11. P. Duwez: *Trans. ASM*, 1953, vol. 45, pp. 934-40.
12. T. Sato, S. Hukai, and Y-C. Huang: *J. Austral. Inst. Met.*, 1960, vol. 5(2), pp. 149-53.
13. D. Kramer and C. G. Rhodes: *Trans. TMS-AIME*, 1967, vol. 236, pp. 1612-15.
14. C. Baker and J. Sutton: *Phil. Mag.*, 1969, vol. 19, pp. 1223-55.
15. V. A. Vozilkin, N. N. Buynov, Yu. F. Bychkov, V. G. Vereshchagin, V. R. Karasik, G. B. Kurganov, and V. A. Mal'tsev: *Phys. Met. Metallog.*, 1970, vol. 30(4), pp. 82-90.
16. A. T. Balcerzak and S. L. Sass: *Metall. Trans.*, 1972, vol. 3, pp. 1601-05.
17. O. Lyon: *J. Less-Common Met.*, 1981, vol. 81, pp. 103-13.
18. D. deFontaine: *Acta Metall.*, 1970, vol. 18, pp. 275-79.
19. H. E. Cook: *Acta Metall.*, 1973, vol. 21(10), pp. 1445-49.
20. H. E. Cook: *Acta Metall.*, 1974, vol. 22(2), pp. 239-47.
21. H. E. Cook: *Acta Metall.*, 1975, vol. 23(9), pp. 1027-39.
22. H. E. Cook: *Acta Metall.*, 1975, vol. 23(9), pp. 1041-54.
23. D. deFontaine, N. E. Paton, and J. C. Williams: *Acta Metall.*, 1971, vol. 19, pp. 1153-62.
24. N. B. D'yakonova, I. V. Lyasotskii, A. I. Zaitsez, and V. V. Luzanov: *Sov. Phys.-Solid State*, 1983, vol. 25(7), pp. 1194-98.
25. D. J. Cometto, G. L. Houze, Jr., and R. F. Hehemann: *Trans. TMS-AIME*, vol. 233, pp. 30-39.
26. D. L. Moffat: Ph.D. Thesis, University of Wisconsin–Madison, 1985.
27. D. C. Larbalestier, A. W. West, W. Starch, W. H. Warnes, P. J. Lee, W. K. McDonald, P. O'Larey, K. Hemachalam, B. Zeitlin, R. Scanlan, and C. Taylor: *IEEE Trans. Mag.*, 1985, vol. MAG-21(2), p. 269.
28. W. K. McDonald: private communication, SC Company, Huntsville, AL, 1985.
29. S. L. Sass: *Acta Metall.*, 1969, vol. 17(7), pp. 813-20.
30. K. K. McCabe and S. L. Sass: *Phil. Mag.*, 1971, vol. 23, pp. 957-70.
31. A. W. West: private communication, Eastman Kodak Co., Rochester, NY, 1987.
32. M. I. Buckett: private communication, Northwestern University, Evanston, IL, 1986.
33. H. Kaneko and Y-C. Huang: *Nippon Kinzoku Gakkai*, 1963, vol. 27(8), pp. 387-93.